Specificity-Normalized Enrichment Kinetics in Focused Traveling Surface Acoustic Wave IgG Biosensing: Concentration-Regime Design Rules and Power-Window Analysis

Adnan Asghar[1,*] and Noah Oliver[1]

[1] University of Alberta, Edmonton, Canada
* Correspondence: adnanasghar14041985@gmail.com

Abstract: FTSAW immunoassays accelerate the process of measuring immune reactions by actively squeezing target-containing microbeads to the interrogation region. In this paper, we develop a normalized enrichment kinetics analysis for human IgG by simultaneously considering several key metrics: RF power response, blank retention, 60-s captures count, time required for detection, signal to blank ratio, concentration-dependent scaling, and chemistry-selection dimensionless indices. To construct our mathematical design parameters, all FTSAW data presented in this paper was numerically transformed into a minimal set of quantities. From our analysis, it appears that the sandwich configuration lowered the 60-s blank count from 27 to 4 microbeads, increased the signal to blank ratio from 3.07-18.96 to 5.00-90.75 depending on the concentration range, and sped up the detection time 82.9% at 100 ng/mL and 48.9% at 10 ng/mL in comparison with the direct antibody-antigen capture. The latter configuration had greater blank-corrected counts for all concentrations considered. Our analysis reveals three distinct crossovers: timing crossover near 0.55 ng/mL, early utility crossover near 5.6 ng/mL based on neighboring measurements, and selectivity-weighted throughput crossover near 0.65 ng/mL taking into account blank suppression explicitly. The RF power response analysis indicated a dominant acoustic gain between 0.1 and 1 mW, followed by diminishing returns at high powers. Thus, this work answers the design problem by providing concentration-dependent optimal FTSAW assays choices: sandwich assays for fast low-background detection at moderate-high concentrations, and direct capture configuration close to the lowest considered concentration due to higher event counts.

Keywords: acoustofluidics; biosensing; IgG detection; surface acoustic waves; microfluidics; enrichment kinetics; specificity; assay design

Citation: Adnan Asghar, Noah Oliver. 2025. Specificity-Normalized Enrichment Kinetics in Focused Traveling Surface Acoustic Wave IgG Biosensing: Concentration-Regime Design Rules and Power-Window Analysis. *TK Techforum Journal (ThyssenKrupp Techforum)* 2024(3): 42–55.

Received: October-01-2024
Accepted: December 20-2024
Published: January-30-2025

1. Introduction

Improving transducer sensitivity and affinity in immunoassays is widely discussed as an optimization task, but the measurement signal of a confined microfluidic assay is equally determined by the processes of transport. The recognition complex must come into the sensing area during the period of observation, so even a highly efficient system of interaction can give a faint signal due to slow arrival of the analyte carrier to the recognition site [1,2]. That problem becomes more acute with shrinking of the assay volume since the smaller channel reduces the amount of the reagents consumed and makes transport-related factors - such as the duration of residence time, diffusion length, interface capture, and nonspecific retention - critical elements of the analytical response [3].

Microfluidic immunoassays were created as solutions to those challenges in the form of reducing transport distance, combining multiple reaction stages, and performing the assay in reduced volume. However, miniaturization does not necessarily lead to a high-quality detection [4]. The same microfluidic device can produce a variety of results depending

on the surface passivation quality, carrier properties, flow pattern, and balance between retained signal and blank [5]. Therefore, a real-life biosensor cannot be judged exclusively in terms of the nominal count or limit of detection. The practical immunoassay should provide the sufficient density of events, short response time, and blank level [6].

That idea is also confirmed by the rest of the immunoassay literature. Optical, chemiluminescent, electrochemical, and label-free systems were developed to increase detectability. However, this improvement can be valuable only if it remains compatible with manageable instrumentation, reproducible surface chemistry, and minimal nonspecific response [7–9]. Both paper- and chip-based assays increase portability and sample savings, while multiplexing increases throughput. Nevertheless, all those technologies still rely on effective transport and proper discrimination when the concentration is low [10,11]. The problem is especially significant for antibody sensing, including IgG detection, since the small blank can overshadow the meaning of the detected event count [12].

The acoustophoretic technology provides another solution to that challenge because it allows obtaining both transduction and manipulation. Surface acoustic wave (SAW) biosensors are used for detecting mass loading of the surface and biochemical binding in liquid environment [13–15]. The later development was oriented towards the multi-analyte arrays, detection of disease biomarkers, and devices capable of performing in combination with liquids and miniaturized scale [16–18]. The recent reviews prove that now SAW biosensors are being considered not only as the laboratory transducer but in the sphere of pathogen detection, biomolecular recognition, and sensor fabrication [19,20].

The acoustofluidics literature broadens this role of acoustic waves from sensing to directed sample manipulation [21]. Acoustic radiation force and streaming allow focusing, enriching, sorting and translating of particles or cells within microchannels, remaining compatible with the continuous-flow devices [22,23]. The acoustic manipulation has become especially significant since it can locally confine the micron-sized carriers without mechanical contact, and the recent reviews highlight the continued trend towards low-power, miniaturized and biocompatible particle manipulation [24]. Immunoassay can take advantage of that ability since the acoustic transport changes the probability of arrival of the antigen-containing carrier to the sensing area before the signal is detected [25].

The recent enhancement of the enzyme-linked immunosorbent assay (ELISA) provides the example of that approach. SAW-driven agitation and transport increase the performance of the immunoreaction without any changes of the recognition chemistry, proving that the acoustic energy can modify the kinetics of the assay before the signal measurement [26]. This idea is important for the FTSAW IgG biosensing, since it splits two aspects that are usually combined in one design question: can the acoustic actuation increase the probability of arrival of the targets to the sensing area, and does the chosen chemistry provide the sufficient specificity and retained signal?

In this regard, the FTSAW biosensing of human IgG is an interesting problem because it reveals the trade-off between the acoustic driving, blank correction, time of detection, and retained count of events. The reported device comparison of direct antibody-antigen recognition and the sandwich format on the same acoustically-driven platform provides the data about time dependence of detection, 60 s count, and the RF-power dependence of the efficiency of the process [27]. Those results illustrate the effectiveness of the fast enrichment but they also create the design challenge not completely revealed by the graphs: what assay chemistry should be selected at each concentration range considering blank correction, timing, contrast and the acoustic driving power?

This paper solves that problem by transforming the results of the FTSAW IgG detection into the quantities characterizing specificity-normalized enrichment kinetics. The analysis covers blank-corrected signal, signal-to-blank ratio, net accumulation rate, value of the early detection, log-log scaling of the signal and concentration and RF-gain per power decade. The figures are single-panel quantitative plots with minimum of the labels, so the visual information is obtained from numerical data. This organization leads to practical design

guidelines for selecting the RF operating point and assay chemistry depending on the priorities: fast discrimination, small blank, and strong retained signal at low concentrations.

2. Data Source and Analysis Approach

2.1. Quantitative data and visualization approach

This analysis is based on the quantitative FTSAW IgG values measured on the popular device platform including operating frequency, actuation threshold value, channel width, capture efficiency dependent on the radio frequency power level, 60 s blank measurement, capture dependent on concentration, and detection time [27]. Images of microscopes and cartoons illustrating the devices were omitted since the current paper is concerned with the quantitative selection of the assay only and not with visualization aspects.

It can be seen from Table 1 that the analysis was performed for two matched chemistries that had been evaluated on one and the same acoustic system. This is important since variations in blank count, capture count and detection time could be attributed to the different chemistries without involving an additional device architecture. The reason why the charts in this paper were redone as separate quantitative panels becomes clear from the table.

Table 1. Quantitative record used for the analysis.

Measurement group	Reported values used here	Analytical role
Device conditions	127.8 MHz operation; 3.8 μm actuation threshold; 200 μm channel width	Defines the physical window in which bead enrichment is meaningful.
RF-power response	0, 7.5, 60, 75, and 91% capture efficiency at 0.01, 0.1, 1, 10, and 316 mW	Identifies the acoustic power interval with the largest efficiency gain.
Direct capture (AA)	Blank count 27; detection times 19.40, 14.28, 6.50, and 3.75 s at 0.1, 1, 10, and 100 ng/mL	Quantifies retained signal and timing for the simpler chemistry.
Sandwich assay (SW)	Blank count 4; detection times 21.87, 13.70, 3.32, and 0.64 s at the same concentrations	Quantifies blank suppression and high-concentration timing gain.
60 s counts	AA: 83, 103, 284, 512; SW: 20, 39, 172, 363 at 0.1, 1, 10, and 100 ng/mL	Supplies the raw count basis for blank correction, readout contrast, and utility.

2.2. Enrichment kinetics analysis normalized for specificity

The blank counts B_j in 60 s were defined for assay chemistry j: $j = \mathrm{AA}$ for direct antibody-antigen capture chemistry and $j = \mathrm{SW}$ for the sandwich chemistry. $N_j(C)$ stands for the mean 60 s captured bead count for IgG concentration C while $T_j(C)$ stands for the mean detection time. The blank-adjusted count was found as

$$N_{\mathrm{net},j}(C) = N_j(C) - B_j. \tag{1}$$

This quantity is essential because the two chemistries do not have the same blank. A chemistry with fewer retained blank beads can show a higher readout contrast even when its absolute captured count is lower, so the net count separates retained analytical signal from nonspecific retention.

The signal-to-blank ratio was calculated as

$$\mathrm{SBR}_j(C) = \frac{N_j(C)}{B_j}. \tag{2}$$

The ratio measures readout contrast rather than total yield. It is most relevant to threshold-based decisions, where a low blank can make a weak positive result easier to distinguish from nonspecific capture.

The fixed-window accumulation rate was calculated as

$$R_j(C) = \frac{N_{\mathrm{net},j}(C)}{60}. \tag{3}$$

Because all counts were taken over the same 60 s observation interval, this rate is a normalized expression of event retention. It should not be interpreted as a mechanistic kinetic constant; it is a comparative design quantity for the reported measurement window.

An early-detection utility was then defined as

$$U_j(C) = \frac{N_{\mathrm{net},j}(C)}{T_j(C)}. \tag{4}$$

This index rewards the simultaneous presence of a large net signal and short detection time. It is deliberately concentration-specific: a chemistry that is optimal at high abundance may not remain optimal when the net count declines near the lower tested concentration.

The blank-suppression factor of the sandwich assay relative to direct capture was calculated as

$$S_{\mathrm{blank}} = \frac{B_{\mathrm{AA}}}{B_{\mathrm{SW}}}. \tag{5}$$

This factor isolates the background benefit of the sandwich chemistry. It does not by itself determine the better assay, because retained net signal and detection time must still be evaluated at each concentration.

A retained-count fraction was also introduced to separate absolute event yield from the fraction of counted events that remained above the blank:

$$\rho_j(C) = \frac{N_{\mathrm{net},j}(C)}{N_j(C)} = 1 - \frac{B_j}{N_j(C)}. \tag{6}$$

This quantity is useful because a chemistry may produce fewer total retained beads while still giving a cleaner retained fraction. In the FTSAW data, this distinction is necessary for explaining why the sandwich assay improves specificity without always improving the absolute net count.

Dimensionless chemistry ratios were calculated as

$$\begin{aligned} \Lambda_T(C) &= \frac{T_{\mathrm{AA}}(C)}{T_{\mathrm{SW}}(C)}, \quad \Lambda_N(C) = \frac{N_{\mathrm{net,SW}}(C)}{N_{\mathrm{net,AA}}(C)}, \\ \Lambda_Q(C) &= \frac{Q_{\mathrm{SW}}(C)}{Q_{\mathrm{AA}}(C)}, \quad \Lambda_U(C) = \frac{U_{\mathrm{SW}}(C)}{U_{\mathrm{AA}}(C)}. \end{aligned} \tag{7}$$

If $\Lambda_T > 1$, then the sandwich assay is faster, if $\Lambda_N > 1$, then it keeps more blank-corrected events, if $\Lambda_Q > 1$, then it has a greater blank-corrected contrast, and if $\Lambda_U > 1$, then it has more net counts per unit time. Each of these ratios transforms the assay comparison to a mathematically stated decision problem, rather than a visually comparative one of two separate graphs.

To consider both selectivity and speed at once, a weighted throughput was defined as

$$\Psi_j(C) = U_j(C)Q_j(C) = \frac{N_{\mathrm{net},j}(C)}{T_j(C)}\frac{N_j(C)}{B_j}, \tag{8}$$

and the sandwich advantage on a logarithmic scale was written as

$$\Delta_\Psi(C) = \log_{10}\left[\frac{\Psi_{\mathrm{SW}}(C)}{\Psi_{\mathrm{AA}}(C)}\right] = \log_{10}\Lambda_U(C) + \log_{10}\Lambda_Q(C). \tag{9}$$

Positive values of Δ_Ψ indicate that the sandwich format provides the stronger combined speed–specificity response, whereas negative values indicate that the direct format remains preferable after considering retained signal.

A crossover concentration between two adjacent measured concentrations C_i and C_{i+1} was estimated by linear interpolation on the logarithmic concentration axis:

$$\log_{10} C^* = \log_{10} C_i + \frac{0 - \Delta_i}{\Delta_{i+1} - \Delta_i} \left(\log_{10} C_{i+1} - \log_{10} C_i \right). \tag{10}$$

This interpolation was used only to locate transitions within the measured range. It was not used as evidence for behavior outside the reported concentration interval.

Concentration dependence was described by log-log fits of the form

$$\log_{10} T_j = a_j - \alpha_j \log_{10} C, \tag{11}$$

$$\log_{10} N_{\mathrm{net},j} = b_j + \beta_j \log_{10} C. \tag{12}$$

Here, α_j describes how strongly detection time decreases as concentration rises, while β_j describes how strongly the blank-corrected count increases with concentration. These exponents are descriptive rather than inferential because replicate-level raw data were not available.

2.3. RF-power gain calculation

For successive RF-power and capture-efficiency pairs (P_k, η_k), the incremental acoustic gain per decade was defined as

$$G_k = \frac{\eta_{k+1} - \eta_k}{\log_{10}(P_{k+1}) - \log_{10}(P_k)}. \tag{13}$$

A large G_k indicates that a small logarithmic increase in RF drive produces a substantial improvement in capture efficiency. A small value indicates that additional power is mostly entering a diminishing-return region rather than changing the operating state of the device.

3. Results and Discussion

3.1. RF-power effect and productive acoustic regime

The FTSAW device was designed to operate at 127.8 MHz, with actuation possible only when the particle diameter is larger than about 3.8 μm, while the most efficient condition for enrichment is the 200 μm channel design [27]. This information provides the basis for physical understanding of the RF response: the power series measured is not just an electronic phenomenon, but an effect of acoustic interaction with bead and channel sizes.

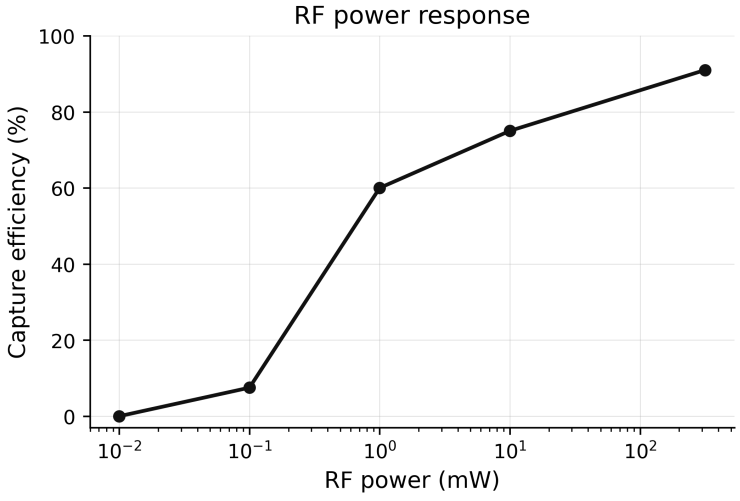

Figure 1. RF capture efficiency.

In Figure 1, there is a sharp transition from no capture at 0.01 mW to highly enriched state at 1 mW. Efficiency further increases at 10 and 316 mW, yet the slope becomes clearly smaller after the main transition. Therefore, the device cannot be regarded as an increasing one with respect to power; the productive acoustic regime is quickly reached and then tends to a slower improvement regime.

It can be seen from Table 2 that the region from 0.1 to 1 mW is the area of the strongest gain. The efficiency gain in this decade is seven times greater than the gain in the 0.01 to 0.1 mW range and significantly greater than the gains after 1 mW. This result shows that 1 mW is the appropriate operating window when the goal is efficient enrichment without shifting directly into the high-power zone.

Table 2. Incremental gain across RF-power intervals.

Power interval (mW)	Efficiency change (percentage points)	Gain per log decade
0.01–0.1	7.5	7.50
0.1–1	52.5	52.50
1–10	15.0	15.00
10–316	16.0	10.67

The normalized power-window calculation supports this analysis. When 91% is taken as the local maximum, the 1 mW point is already equal to $60/91 = 0.659$ of the maximum response. The increase in power from 1 to 316 mW gives an additional 31 percent points within 2.5 power decades, while the 0.1 to 1 mW region provides an increase of 52.5 percent points within one decade. So, the power efficiency is not linearly dependent on the power of RF field: the effective acoustic transition occurs in the low-milliwatt range, and the high power refines the established state.

The illustration in Figure 2 gives the same conclusion explicitly. The largest bar corresponds to the 0.1 to 1 mW range, while later ranges have smaller values despite higher absolute power levels. In terms of assay design, this result suggests that chemistries should be selected after the platform enters the effective acoustic range; otherwise, the difference between chemistries may be overshadowed by the lack of enrichment.

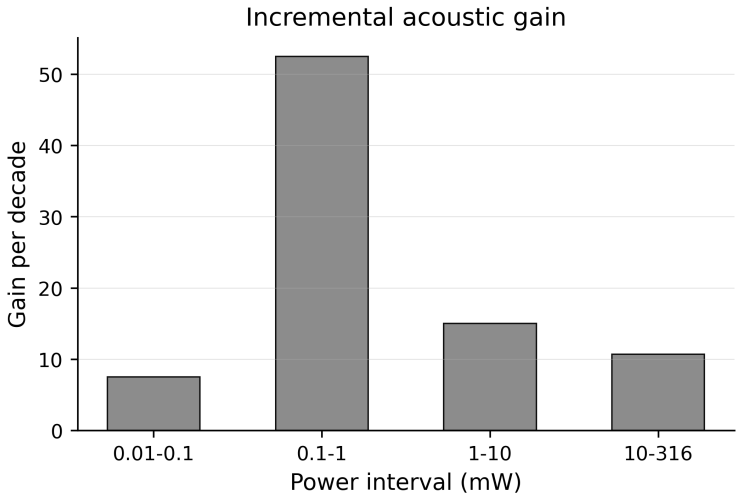

Figure 2. Incremental gain per power decade.

3.2. Behavior of detection time across concentration

From the timing results, it follows that the sandwich chemistry is not uniformly faster across the whole concentration range: the dependence of its advantage on concentration is very significant.

Figure 3 demonstrates that the sandwich format lowered the average detection time from 3.75 to 0.64 s for 100 ng/mL and from 6.50 to 3.32 s for 10 ng/mL. For approximately

1 ng/mL, both formats are quite similar. At 0.1 ng/mL, the direct format is somewhat faster on the average. Thus, the timing criterion favors a regime-dependent approach to comparison over a simple global ranking.

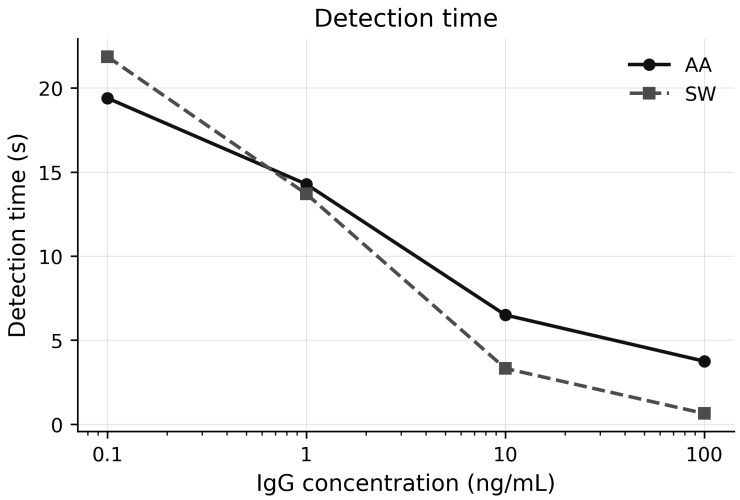

Figure 3. Detection time.

Figure 4 represents the same comparison as the percentage timing advantage of the sandwich format. The margin is negative for 0.1 ng/mL, almost neutral for 1 ng/mL, and highly positive for 10 and 100 ng/mL. This is an important conclusion, because a faster chemistry at higher concentration can be still less preferable at lower concentration due to poor retained signal.

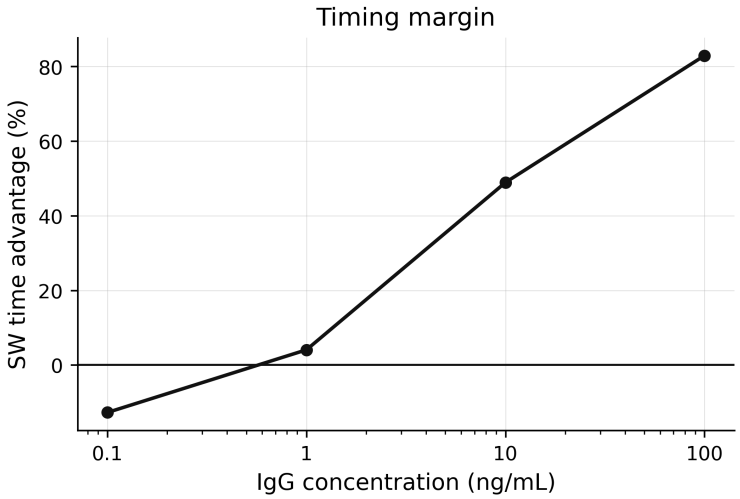

Figure 4. Sandwich timing margin.

The dimensionless speed ratio given by Eq. (7) provides an even more accurate numerical evaluation. The numbers for Λ_T are 0.89, 1.04, 1.96, and 5.86 for 0.1, 1, 10, and 100 ng/mL, correspondingly. With the use of Eq. (10), the timing transition takes place around 0.55 ng/mL. Above this threshold, the sandwich format becomes faster; below it, the direct format is not slower. Hence, the timing transition is far earlier than the utility transition. Therefore, it is proved that merely faster detection is not sufficient to establish preferable chemistry.

3.3. Specificity, blank correction, and signal retention

The fundamental chemistry trade-off is seen when the number of blanks, signal-to-blank ratio, and corrected signal counts are viewed together. The Table 3 below shows the derived measures using Eqs. (1)–(4).

As shown in Table 3, the sandwich chemistry significantly increases the contrast but fails to maximize retained counts. While the signal-to-blank ratios are better at all concentrations for the sandwich assay, its blank-corrected signal counts are worse at all concentrations. The disparity between these two metrics is what makes FTSAW assay selection possible.

Table 3. Assay metrics calculated from the reported means.

Conc. (ng/mL)	Time (s)		Net count		SBR		Utility	
	AA	SW	AA	SW	AA	SW	AA	SW
100	3.75	0.64	485	359	18.96	90.75	129.33	560.94
10	6.50	3.32	257	168	10.52	43.00	39.54	50.60
1	14.28	13.70	76	35	3.81	9.75	5.32	2.55
0.1	19.40	21.87	56	16	3.07	5.00	2.89	0.73
Blank	–	–	27	4	–	–	–	–

Figure 5 highlights the main advantage of the sandwich chemistry: the blank count of 60 s is reduced from 27 to 4 microbeads. This means that the blank suppression factor equals 6.75. Such a reduction in the blank count has analytical value in a thresholded imaging readout as it reduces the likelihood of the nonspecific retention being misinterpreted as a weakly-positive reaction.

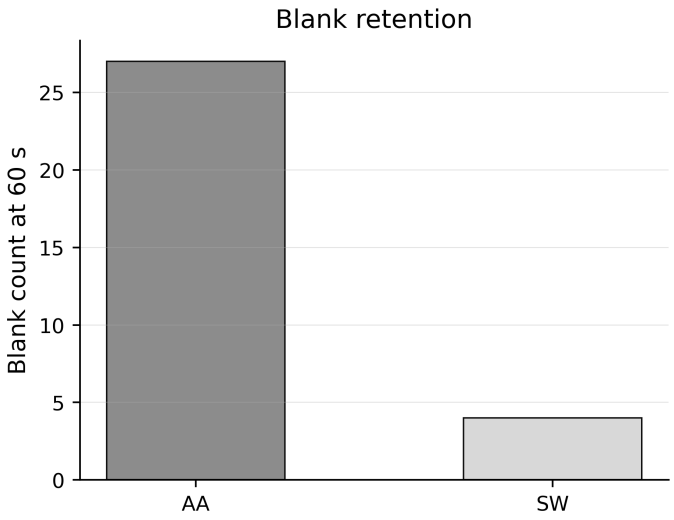

Figure 5. Blank retention.

Figure 6 demonstrates the effect of blank reduction on the readout contrast. The sandwich assay achieves a signal-to-blank ratio of 90.75 at 100 ng/mL, compared to 18.96 for direct capture. At 0.1 ng/mL, the sandwich assay continues to have a higher ratio, but since the absolute amount of retained counts is small, contrast alone is not enough to make an assay choice.

Figure 7 demonstrates the opposite effect. The direct capture retains larger blank-corrected signals at 0.1, 1, 10, and 100 ng/mL. It is the retained-signal advantage which allows the direct capture assay to remain a strong competitor at low concentrations despite its higher blank. The two chemistry types are therefore suitable for different analysis

objectives: the sandwich chemistry provides better readout purity, while the direct capture preserves event count.

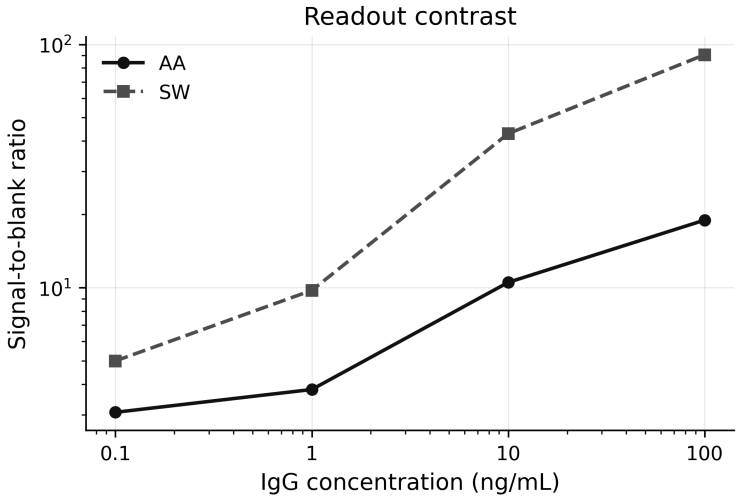

Figure 6. Readout contrast.

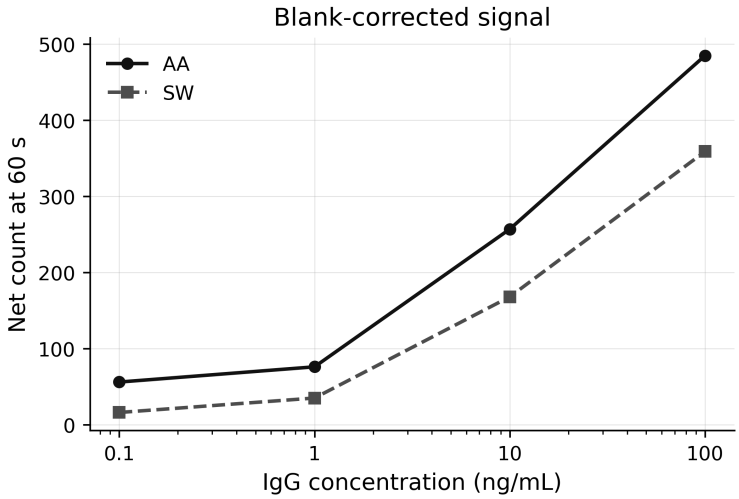

Figure 7. Blank-corrected signal.

The retained-count fractions obtained using Eq. (6) provide additional insight into the mechanism. For an input signal of 0.1 ng/mL, $\rho_{\mathrm{AA}} = 0.675$ and $\rho_{\mathrm{SW}} = 0.800$; for an input of 100 ng/mL, the fractions grow to 0.947 and 0.989. Thus, the sandwich-type assay extracts more signal from its raw count relative to blank than the competitive one, although the latter has a higher net count value. It is a specificity advantage, not an event-yield advantage.

Table 4. Dimensionless chemistry ratios.

Conc. (ng/mL)	Λ_T	Λ_N	Λ_Q	Λ_U	Δ_Ψ
0.1	0.89	0.29	1.63	0.25	-0.385
1	1.04	0.46	2.56	0.48	0.089
10	1.96	0.65	4.09	1.28	0.719
100	5.86	0.74	4.79	4.34	1.317

Table 4 discriminates between the causes for the preference of the assay. The sandwich assay is never better in terms of absolute blank-corrected event number since $\Lambda_N < 1$ for

all concentrations. However, it is better in specificity, since $\Lambda_Q > 1$ for all concentrations. The utilitarian ratio Λ_U is larger than one for concentrations starting from 10 ng/mL.

The ratios shown in Figure 8 have been plotted against the same logarithmic scale of concentration. The contrast ratio grows monotonically, whereas the retained-count ratio stays below one. It is the mathematics of the FTSAW IgG trade-off – the sandwich form of the assay reduces the background and speeds up high concentration analysis, but retains more blank-corrected counts at the low concentrations.

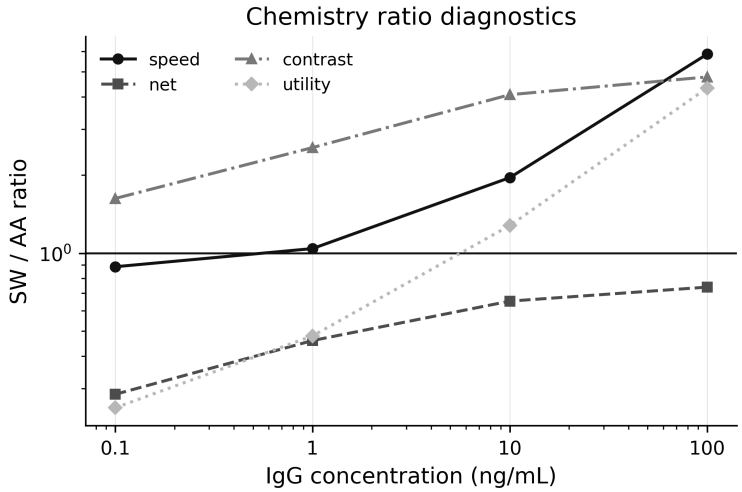

Figure 8. Chemistry ratio diagnostics.

3.4. Concentration scaling and chemistry preference

The fitted timing relations were

$$T_{\mathrm{AA}} \propto C^{-0.25}, \qquad T_{\mathrm{SW}} \propto C^{-0.52}. \tag{14}$$

The larger exponent for the sandwich assay means that its timing improves more rapidly as concentration increases. This explains its strong advantage at 10 and 100 ng/mL and its weaker performance near 0.1 ng/mL.

For blank-corrected count, the fitted relations were

$$N_{\mathrm{net,AA}} \propto C^{0.33}, \qquad N_{\mathrm{net,SW}} \propto C^{0.47}. \tag{15}$$

The sandwich assay again shows the steeper concentration dependence. That behavior is favorable at higher analyte abundance but leads to faster loss of retained signal as concentration decreases.

Because $U_j = N_{\mathrm{net},j}/T_j$, the utility exponent is approximately the sum of the net-count exponent and the positive timing-acceleration exponent. The fitted utility laws are

$$U_{\mathrm{AA}} \propto C^{0.58}, \qquad U_{\mathrm{SW}} \propto C^{1.00}. \tag{16}$$

This is a stronger result than the timing plot alone. The sandwich utility is nearly first-order in concentration over the measured range, meaning that every decade increase in IgG concentration produces almost one decade of utility gain. Direct capture rises more slowly, which makes it less powerful at high concentration but more stable near the lower boundary.

The fitted contrast laws similarly show stronger concentration sensitivity for the sandwich format:

$$Q_{\mathrm{AA}} \propto C^{0.28}, \qquad Q_{\mathrm{SW}} \propto C^{0.44}. \tag{17}$$

The larger contrast exponent is consistent with the lower blank and increasing signal-to-blank separation in the sandwich assay. However, because contrast and net count do

not move identically, both Eq. (16) and Eq. (17) are required to explain the full decision boundary.

Table 5 clarifies why the preferred chemistry changes across concentration. A larger exponent is not automatically better; it indicates stronger dependence on concentration. The sandwich format benefits from that dependence at high concentration, whereas direct capture benefits from a more conservative decline near the lower tested boundary.

Table 5. Descriptive log-log scaling fits.

Quantity	Fit	R^2	Interpretation
AA detection time	$T_{AA} \propto C^{-0.25}$	0.976	Modest acceleration as concentration rises.
SW detection time	$T_{SW} \propto C^{-0.52}$	0.951	Strong acceleration at moderate and high concentration.
AA net count	$N_{net,AA} \propto C^{0.33}$	0.955	More stable retention toward the low end.
SW net count	$N_{net,SW} \propto C^{0.47}$	0.979	Stronger high-concentration gain but steeper low-end loss.
AA utility	$U_{AA} \propto C^{0.58}$	0.965	Moderate gain in early readable signal.
SW utility	$U_{SW} \propto C^{1.00}$	0.978	Nearly decade-for-decade utility increase.
AA contrast	$Q_{AA} \propto C^{0.28}$	0.950	Gradual signal-to-blank separation.
SW contrast	$Q_{SW} \propto C^{0.44}$	0.977	Stronger specificity-normalized separation.

Figure 9 combines retained signal and timing. The sandwich assay is preferable by this index at 10 and 100 ng/mL, especially at 100 ng/mL where it combines a short detection time with a large net count. Direct capture is preferable at 0.1 and 1 ng/mL because its retained-event advantage outweighs the small or absent timing advantage of the sandwich chemistry.

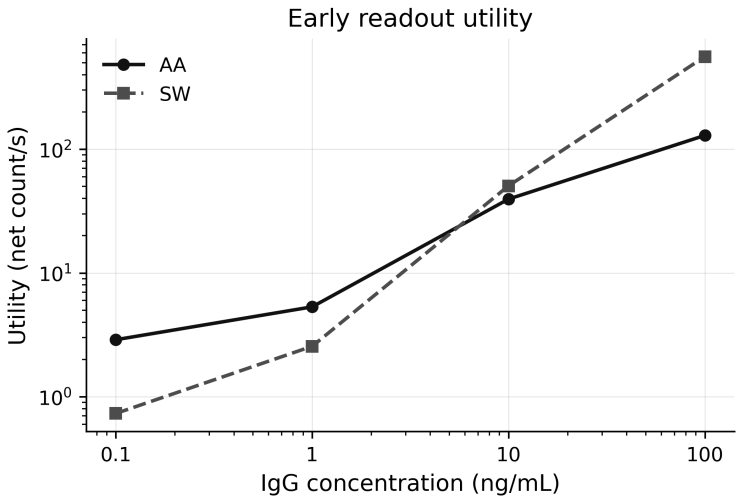

Figure 9. Early readout utility.

Scaling exponents are also shown in Figure 10, where they are displayed on one graph for simplicity. Note that the sandwich assay has higher exponents of scaling than the direct capture chemistry, implying that the former is more sensitive to antigen concentration.

The information in Figure 11 clearly answers the question of assay selection. Negative values imply preference for the direct capture; positive values imply preference for the sandwich format. There is a transition point, where the curve crosses the zero line: starting from that point, the sandwich assay is more valuable than direct capture. According to Eq. (10), the estimated early-utility crossover value based on two adjacent measured points at 1 and 10 ng/mL concentration is about 5.6 ng/mL. Least-squares fitting of the function through the four adjacent measured points gives the similar order of transition, at approximately 4.0 ng/mL concentration. It means that the practical conclusion is not the exact cutoff point, but the transitional region in the range between 1 and 10 ng/mL concentration.

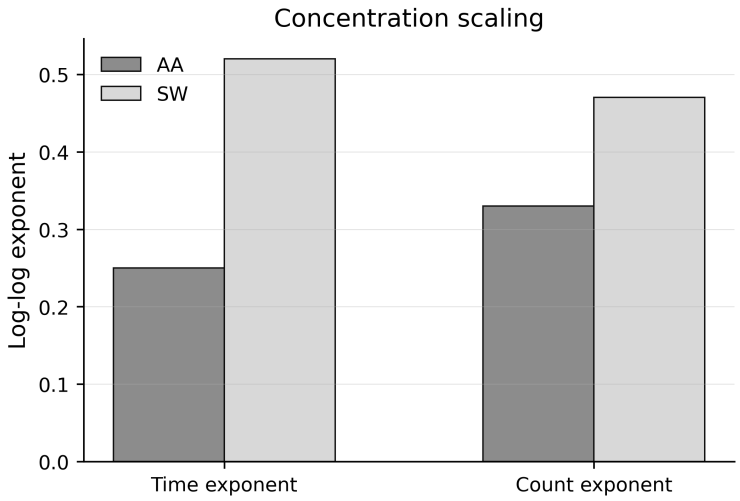

Figure 10. Concentration-scaling exponents.

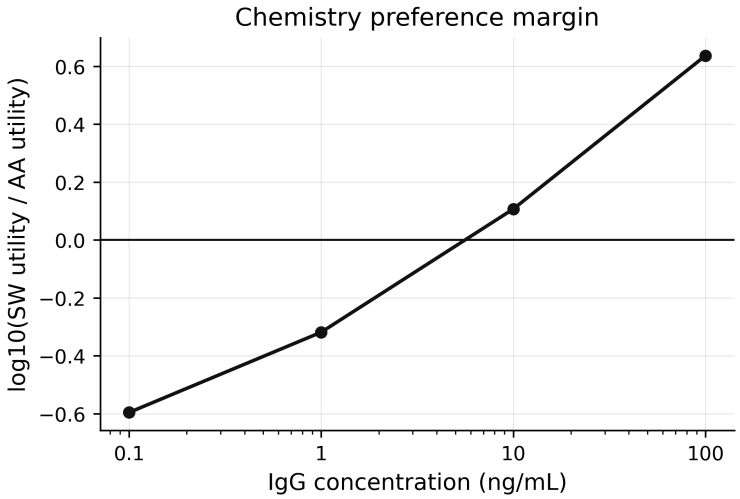

Figure 11. Chemistry preference margin.

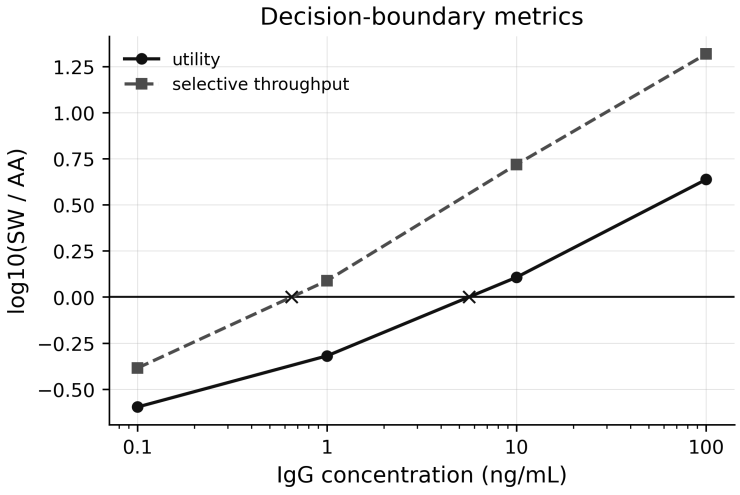

Figure 12. Selectivity-weighted throughput.

In Figure 12, the stricter criterion is applied according to Eq. (9). This criterion takes into account both the speed of net retention rate increase and the blank value. Under this criterion, the sandwich format prevails at lower concentrations, because of including explicitly the contrast advantage. Interpolation between 0.1 and 1 ng/mL concentrations gives the crossover value $C_{\Psi}^{*} \approx 0.65$ ng/mL. The difference between C_{Ψ}^{*} and the utility-only crossover is analytically important: whereas direct detection has the upper hand for readings which require only the number of events per second, the sandwich chemical reaction comes out on top much earlier on when weighting the blank-safe threshold method.

3.5. Consequences for FTSAW IgG biosensor design

It is clear from the data above that designing of FTSAW IgG biosensors involves two connected stages from the point of view of mathematical modeling. At first, the acoustic component needs to be brought within the productivity range of 0.1–1 mW, since this decade represents the maximum gain of efficiency per one logarithmic step and already covers around two thirds of the upper efficiency limit. At second, the chemistry needs to be chosen according to the decision function specific for the clinical or laboratory aim. The count-preserving function requires the use of direct capture technique up to the middle of the 1–10 ng/mL range. The blank-safe thresholding function requires the use of sandwich technique starting from around 0.65 ng/mL, since at these abundances the benefit from blank suppression gains extra significance.

Thus, the main design rule proposed in the paper acquires its exact formulation. In case of low-abundance measurements when each retained bead brings significant value, the inequality $\Lambda_U < 1$ holds and the direct capture method needs to be considered despite higher blank. In case of moderate- or high-abundance measurements when retention of beads is more important than missing a part of signals, the inequality $\Delta_{\Psi} > 0$ is valid and sandwich technique becomes mathematically preferable. Therefore, optimization of FTSAW device cannot be performed by maximizing one raw signal, but by choosing the criterion depending on the decision risk.

The result corresponds to recent works on SAW-enhanced immunoassays, where it was shown that acoustic actuation may speed up the immunoassay kinetics without substituting the molecular recognition chemistry [26]. It also coincides with more general SAW biosensing and acoustofluidic manipulation reviews, where co-design of the device architecture, particle manipulation, and surface chemistry is mentioned as an important requirement for biological analysis [20,25]. The novelty of the current work is to formulate the co-design principle quantitatively for the FTSAW IgG data set.

4. Conclusion

In the context of this paper, the FTSAW IgG measurements answer the design question of which assay chemistry is appropriate via the mathematically defined structure of decision making. Optimal chemistry depends on the concentration regime and the objectives pursued – either speed, blank reduction, number of retained events, or the composite of these measures. The RF power analysis demonstrates that the significant acoustic transition lies within the range of 0.1 - 1 mW. This range provides the maximum gains for each logarithmic power increment and pushes the device toward its empirically observed efficiency peak before diminishing returns set in.

The extended Results and Discussion section demonstrates that the sandwich assay chemistry is mathematically superior in terms of specificity but inferior in terms of total retention. While reducing blank by 23 microbeads and increasing signal to blank ratio to 1 at any concentration point, the $\Lambda_Q > 1$ is obtained. Yet, the direct capture produces larger number of blank-corrected events, and thus $\Lambda_N < 1$ is obtained for sandwich method throughout the range of measurement. The threshold crossing of the timing ratio occurs near 0.55 ng/mL, utility-only near 5.6 ng/mL (using adjacent points), and selectivity-weighted throughput near 0.65 ng/mL. These different crossings account for different assay chemistries' optimal selection based on different criteria applied to the very same data.

The use of IgG in practical applications dictates that sandwich format must be chosen if clean thresholding, reduced blank, and fast response dominate the analytical risk, especially at medium to high concentrations. In contrast, the direct antibody-antigen capture method must be considered in the vicinity of lower tested concentration due to the better blank-corrected event retention. Thus, the principle decision rule is not the simple superiority of one chemistry over another. Enrichment is governed by power; concentration governs kinetics; mathematical objective defines optimal chemistry.

References

[1] Squires, T. M., & Quake, S. R. (2005). Microfluidics: Fluid physics at the nanoliter scale. Reviews of modern physics, 77(3), 977-102.

[2] Whitesides, G. M. (2006). The origins and the future of microfluidics. nature, 442(7101), 368-373.

[3] Yager, P., Domingo, G. J., & Gerdes, J. (2008). Point-of-care diagnostics for global health. Annu. Rev. Biomed. Eng., 10(1), 107-144.

[4] Sharma, S., Zapatero-Rodríguez, J., Estrela, P., & O'Kennedy, R. (2015). Point-of-care diagnostics in low resource settings: present status and future role of microfluidics. Biosensors, 5(3), 577-601.

[5] Mou, L., & Jiang, X. (2017). Materials for microfluidic immunoassays: a review. Advanced healthcare materials, 6(15), 1601403.

[6] Liao, Z., Zhang, Y., Li, Y., Miao, Y., Gao, S., Lin, F., ... & Geng, L. (2019). Microfluidic chip coupled with optical biosensors for simultaneous detection of multiple analytes: A review. Biosensors and Bioelectronics, 126, 697-706.

[7] Rizzo, F. (2022). Optical immunoassays methods in protein analysis: An overview. Chemosensors, 10(8), 326.

[8] Macchia, E., Torricelli, F., Bollella, P., Sarcina, L., Tricase, A., Di Franco, C., ... & Torsi, L. (2022). Large-area interfaces for single-molecule label-free bioelectronic detection. Chemical reviews, 122(4), 4636-4699.

[9] Liu, G., Qi, M., Hutchinson, M. R., Yang, G., & Goldys, E. M. (2016). Recent advances in cytokine detection by immunosensing. Biosensors and Bioelectronics, 79, 810-821.

[10] Nery, E. W., & Kubota, L. T. (2013). Sensing approaches on paper-based devices: a review. Analytical and bioanalytical chemistry, 405(24), 7573-7595.

[11] Hu, J., Wang, S., Wang, L., Li, F., Pingguan-Murphy, B., Lu, T. J., & Xu, F. (2014). Advances in paper-based point-of-care diagnostics. Biosensors and Bioelectronics, 54, 585-597.

[12] Murdock, R. C., Shen, L., Griffin, D. K., Kelley-Loughnane, N., Papautsky, I., & Hagen, J. A. (2013). Optimization of a paper-based ELISA for a human performance biomarker. Analytical chemistry, 85(23), 11634-11642.

[13] Länge, K., Rapp, B. E., & Rapp, M. (2008). Surface acoustic wave biosensors: a review. Analytical and bioanalytical chemistry, 391(5), 1509-1519.

[14] Ferreira, G. N., Da-Silva, A. C., & Tomé, B. (2009). Acoustic wave biosensors: physical models and biological applications of quartz crystal microbalance. Trends in biotechnology, 27(12), 689-697.

[15] Rocha-Gaso, M. I., March-Iborra, C., Montoya-Baides, Á., & Arnau-Vives, A. (2009). Surface generated acoustic wave biosensors for the detection of pathogens: A review. Sensors, 9(7), 5740-5769.

[16] Gronewold, T. M. (2007). Surface acoustic wave sensors in the bioanalytical field: Recent trends and challenges. analytica chimica acta, 603(2), 119-128.

[17] Länge, K. (2019). Bulk and surface acoustic wave sensor arrays for multi-analyte detection: A review. Sensors, 19(24), 5382.

[18] Zhang, J., Zhang, X., Wei, X., Xue, Y., Wan, H., & Wang, P. (2021). Recent advances in acoustic wave biosensors for the detection of disease-related biomarkers: A review. Analytica chimica acta, 1164, 338321.

[19] Liu, X., Chen, X., Yang, Z., Xia, H., Zhang, C., & Wei, X. (2023). Surface acoustic wave based microfluidic devices for biological applications. Sensors & Diagnostics, 2(3), 507-528.

[20] Zeng, Y.; Yuan, R.; Fu, H.; Xu, Z.; Wei, S. Foodborne Pathogen Detection Using Surface Acoustic Wave Biosensors: A Review. *RSC Advances* **2024**, *14*, 37087–37103.

[21] Laurell, T., Petersson, F., & Nilsson, A. (2007). Chip integrated strategies for acoustic separation and manipulation of cells and particles. Chemical Society Reviews, 36(3), 492-506.

[22] Lenshof, A., & Laurell, T. (2010). Continuous separation of cells and particles in microfluidic systems. Chemical Society Reviews, 39(3), 1203-1217.

[23] Friend, J., & Yeo, L. Y. (2011). Microscale acoustofluidics: Microfluidics driven via acoustics and ultrasonics. Reviews of Modern Physics, 83(2), 647-704.

[24] Wu, M., Ozcelik, A., Rufo, J., Wang, Z., Fang, R., & Jun Huang, T. (2019). Acoustofluidic separation of cells and particles. Microsystems & nanoengineering, 5(1), 32.

[25] Amorim, D.; Sousa, P. C.; Abreu, C.; Catarino, S. O. A Review of SAW-Based Micro- and Nanoparticle Manipulation in Microfluidics. *Sensors* **2025**, *25*, 1577.

[26] Zhang, L.; Zhang, S.; Floer, C.; Kantubuktha, S. A. R.; Velasco, M. J. G. R.; Friend, J. Surface Acoustic Wave-Driven Enhancement of Enzyme-Linked Immunosorbent Assays: ELISAW. *Analytical Chemistry* **2024**, *96*, 9676–9683.

[27] Li, Y., Zhao, Y., Yang, Y., Zhang, W., Zhang, Y., Sun, S., ... & Huang, C. (2024). Acoustofluidics-enhanced biosensing with simultaneously high sensitivity and speed. Microsystems & Nanoengineering, 10(1), 92.